Expanded View Figures

Figure EV1. Features of the hLRRC8C mutant V390L.

Comparison of the highest resolved cryo-EM maps (contoured at 8σ) obtained from the hLRRC8C^{V390L} and hLRRC8C^{WT} datasets. (**A**) Cryo-EM map of hLRRC8C^{V390L} (top) and hLRRC8C^{WT} (bottom) superimposed on indicated subunits. (**B**) hLRRC8C^{V390L} (left) and hLRRC8C^{WT} (right) densities viewed from the cytoplasm. (**A**, **B**) Parts of protein subunits that are defined in the density are shown as ribbons, subunit numbering is as in Fig. 3D, E.

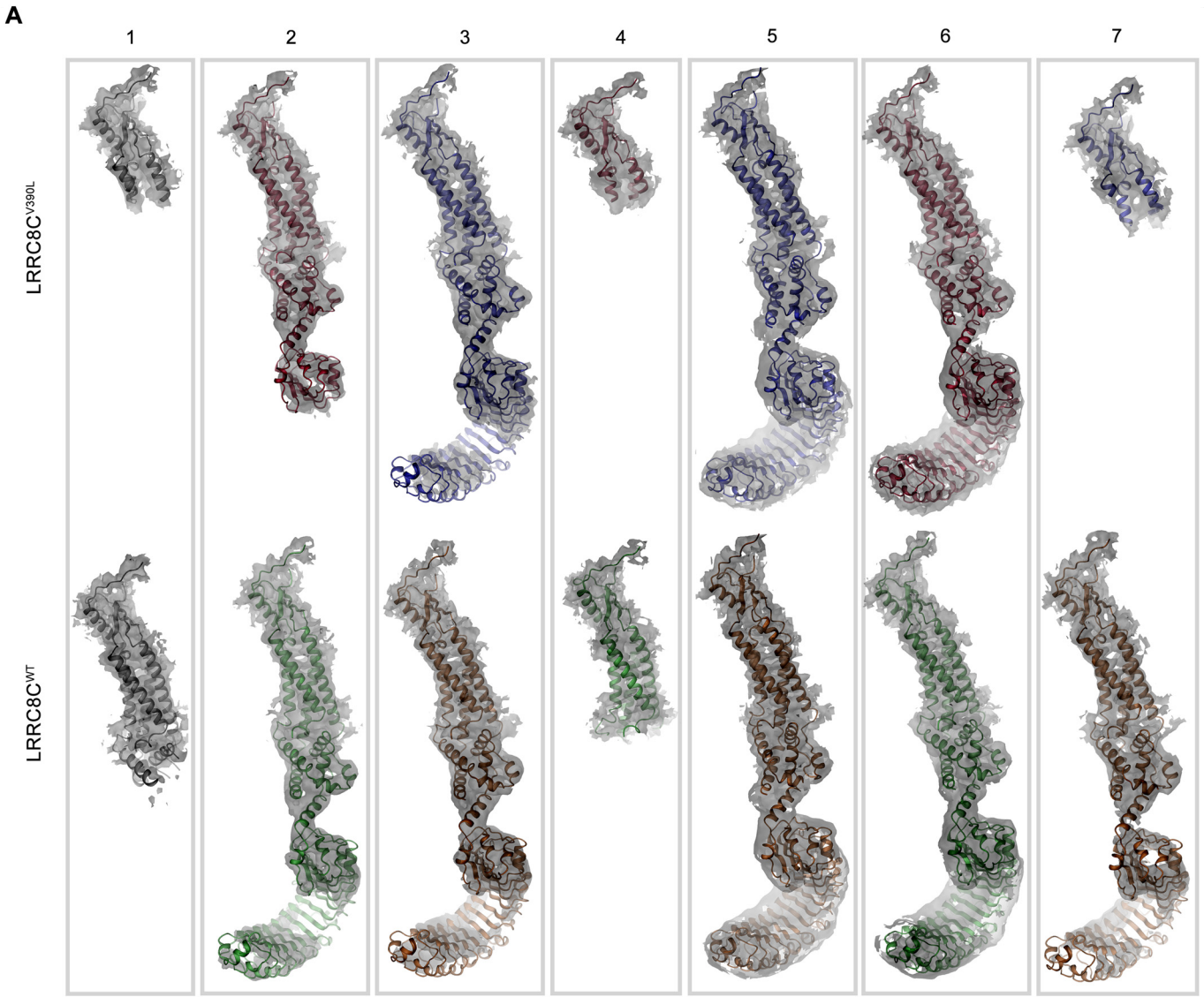
A
1
2
3
4
5
6
7
LRRC8C^V390L
LRRC8C^WT

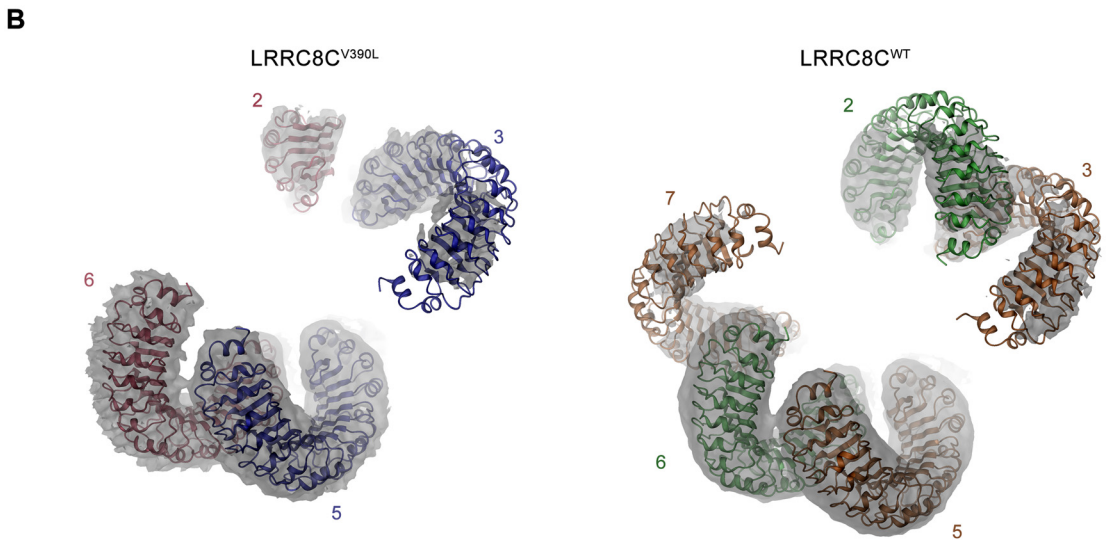
B
LRRC8C^V390L
2
3
6
5
LRRC8C^WT
2
3
7
6
5

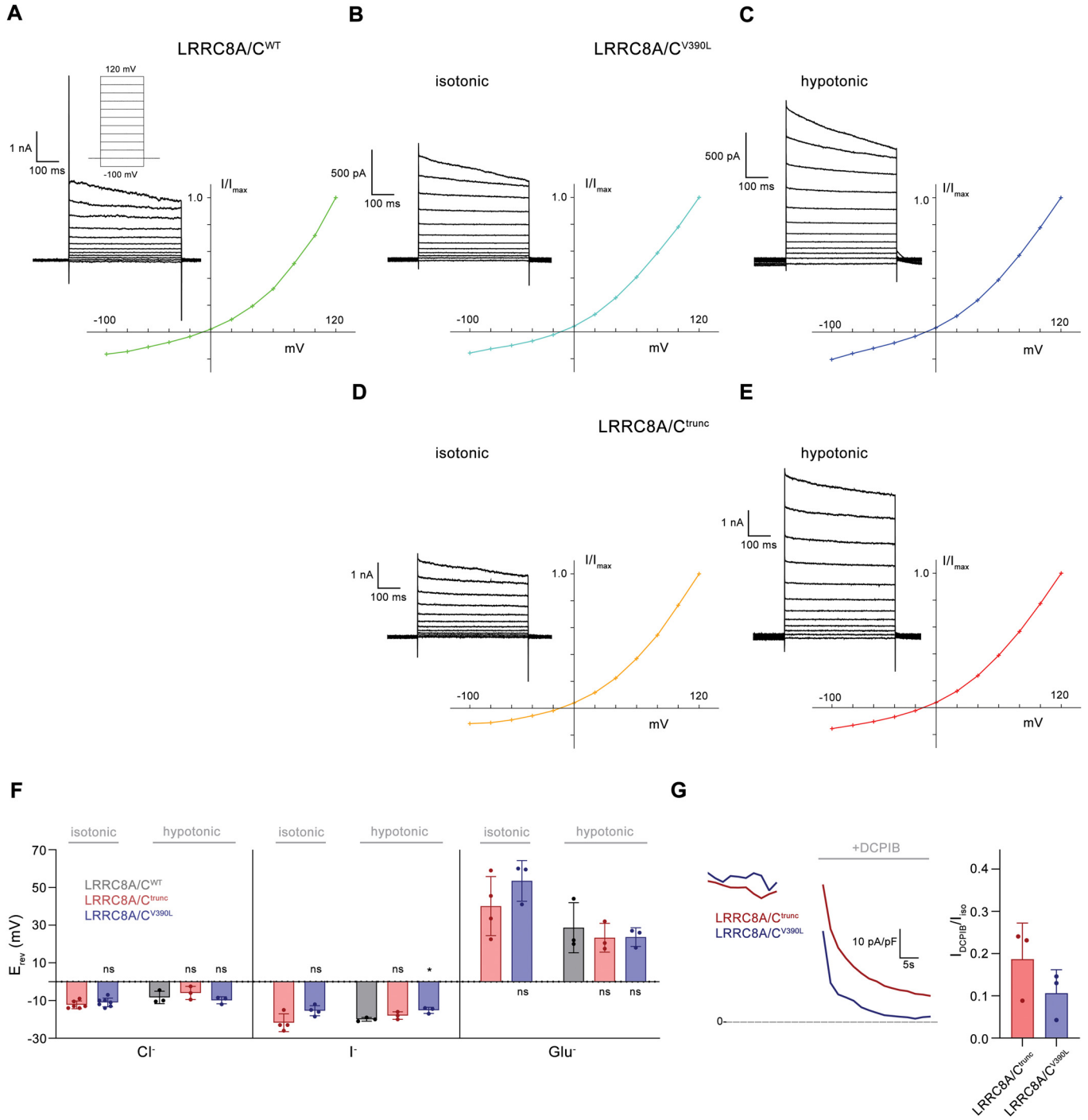
A
LRRC8A/C^WT
120 mV
-100 mV
1 nA
100 ms
I/I_max
1.0
-100
120
mV
B
LRRC8A/C^V390L
isotonic
500 pA
100 ms
C
hypotonic
D
LRRC8A/C^trunc
isotonic
E
hypotonic
F
isotonic
hypotonic
LRRC8A/C^WT
LRRC8A/C^trunc
LRRC8A/C^V390L
E_rev (mV)
70
50
30
10
-10
-30
ns
*
Cl-
I-
Glu-
G
+DCPIB
10 pA/pF
5s
I_DCPIB/I_iso
0.4
0.3
0.2
0.1
0.0

Figure EV2. Functional properties of hLRRC8C mutants in buffer set Δsalt.

(**A**) Representative current traces and current–voltage relationship of an LRRC8$^{-/-}$ cell transfected with constructs coding for hLRRC8A and hLRRC8C^{WT} after swelling of cells in buffer set Δsalt showing the expected features of an LRRC8A/C channel. (**B**, **C**) Representative current traces and current–voltage relationships of an LRRC8$^{-/-}$ cell transfected with constructs coding for hLRRC8A and hLRRC8C^{V390L} under isotonic (**B**) and hypertonic conditions (**C**). (**D**, **E**) Representative current traces and current–voltage relationships of an LRRC8$^{-/-}$ cell transfected with constructs coding for hLRRC8A and hLRRC8C^{trunc} under isotonic (**D**) and hypertonic conditions (**E**). The similar general properties of currents obtained under isotonic and hypotonic conditions with respect to the negative reversal potential, the pronounced outward rectification and the inactivation at strongly positive voltages show characteristics of VRACs composed of LRRC8A and C-subunits. (**A–E**) Currents were recorded by patch-clamp electrophysiology in the whole-cell configuration upon perfusion of cells with either isotonic (**B**, **D**) or hypotonic buffer (**A**, **C**, **E**, described in "Methods"). Normalized IV-plots are displayed (right, bottom). Voltage protocol is as shown in (**A**). (**F**) Reversal potentials of currents mediated by LRRC8A/C^{trunc} or LRRC8A/C^{V390L} in isotonic and hypotonic conditions of buffer system 1 (Δsalt) in comparison to LRRC8A/C^{WT} currents measured in hypotonic conditions of the same buffer system. Cl^- refers to standard solutions, I^- and Glu^- to solutions where NaCl was replaced by equimolar amounts of NaI or NaGlu, respectively. Due to the lower anion concentration, reversal potentials are generally lower in hypotonic solutions. Panels show measurements of individual cells (spheres), bars represent mean currents, errors are s.e.m. Asterisks indicate significant deviations from WT in the respective conditions in a Brown–Forsythe and Welch's ANOVA test with Dunnett's T3 multiple comparison testing in case of the comparison of currents in hypotonic conditions and deviations from LRRC8C^{trunc} in a unpaired *t* test with Welsch's correction in case of isotonic conditions. Differences were usually not statistically significant (ns) except for one case (*$P = 0.0375$). (**G**) Inhibition of endogenous currents of LRRC8A/C^{trunc} and LRRC8A/C^{V390L} in response to perfusion of isotonic solutions of buffer condition Δsalt containing 50 μM DCPIB. Left, current decrease in representative traces in response to inhibitor addition measured at 100 mV by a ramp protocol. Dashed line refers to zero current. Right, fraction of inhibition of basal currents from respective constructs in response to DCPIB application. Measurements of individual cells are shown as spheres, bars represent mean currents, errors are s.e.m.

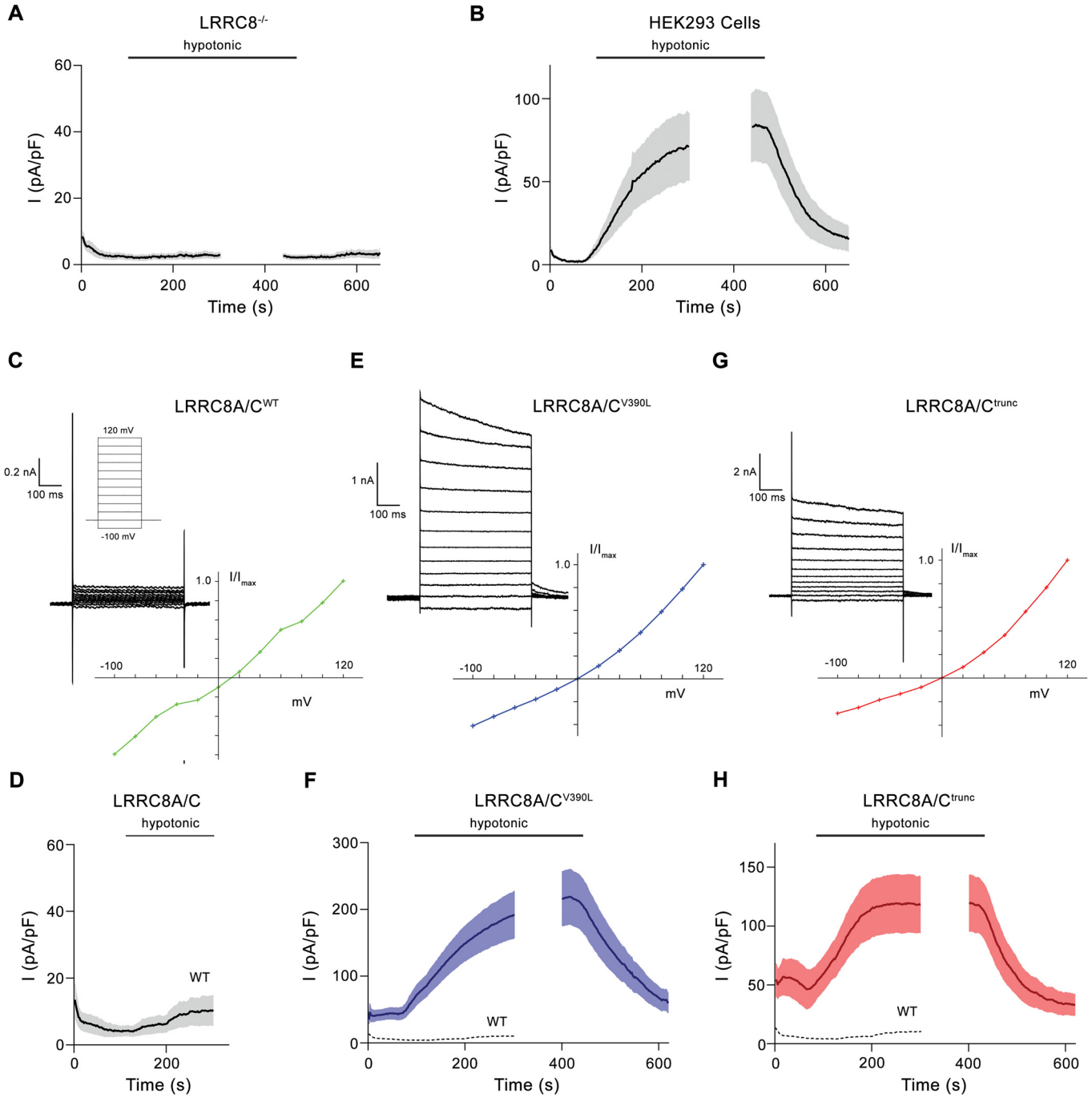

Figure EV3. Functional properties of hLRRC8C mutants in buffer set Δmannitol.

(**A**, **B**) Mean current density (at 100 mV) of LRRC8A$^{-/-}$ cells ($n = 10$) (**A**) and HEK293 cells ($n = 8$) (**B**) recorded in buffer set Δmannitol. (**C**) Representative current traces and current–voltage relationship of LRRC8$^{-/-}$ cells transfected with constructs coding for hLRRC8A and hLRRC8C^{WT} after swelling of cells in buffer set Δmannitol not leading to channel activation. (**D**) Mean current density (at 100 mV) of hLRRC8A/C^{WT} channels ($n = 12$) recorded in buffer set Δmannitol. (**E**) Representative current traces and current–voltage relationship of LRRC8$^{-/-}$ cells transfected with constructs coding for hLRRC8A and hLRRC8C^{V390L} after swelling of cells in buffer set Δmannitol. (**F**) Mean current density (at 100 mV) of hLRRC8A/C^{V390L} ($n = 11$) recorded in buffer set Δmannitol. (**G**) Representative current traces and current–voltage relationship of LRRC8$^{-/-}$ cells transfected with constructs coding for hLRRC8A and hLRRC8C^{trunc} after swelling of cells in buffer set Δmannitol. (**H**) Mean current density (at 100 mV) of hLRRC8A/C^{trunc} channels ($n = 10$) recorded in buffer set Δmannitol. (**A–H**) Currents were recorded by patch-clamp electrophysiology in the whole-cell configuration. Cannels were activated by perfusion of cells with hypotonic buffers (described in methods). (**C**, **E**, **G**) Normalized IV-plots are displayed (right, bottom). Voltage protocol is as shown in (**C**). (**F**, **H**) The mean current of WT is shown as dashed line for comparison. (**D**, **F**, **H**) Panels show mean of indicated number of biological replicates, errors are s.e.m. Note the different scale of the y-axis in the three panels.

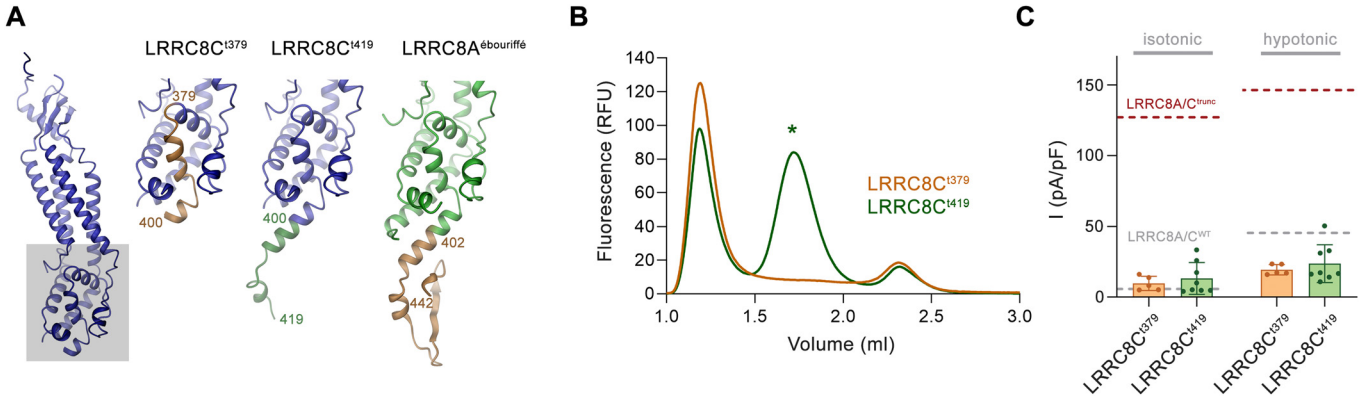

Figure EV4. Biochemical and functional characterization of the constructs LRRC8C^{t379} and LRRC8C^{t419}.

(**A**) Models of truncated LRRC8 constructs. A ribbon representation of LRRC8C^{trunc} is shown left as reference. The gray box indicates the region of interest in different constructs shown to the right: Center left, LRRC8C^{t379}, the region on the C-terminus of LRRC8C^{trunc} (380–400) that is absent in this construct is highlighted in orange; Center right, LRRC8C^{t419}, the sequence extension compared to LRRC8C^{trunc} (residues 401–419) is highlighted in green; Right, equivalent region of the LRRC8A mutant found in ébouriffé mice (which is truncated after residue 442), with the extension compared to LRRC8C^{trunc} highlighted in orange. (**B**) Fluorescence size exclusion chromatogram of GFP-fusions of the constructs LRRC8C^{t379} and LRRC8C^{t419} after extraction in detergent. Asterisk corresponds to the volume of the heptameric channel. While no oligomer is detected in case of the shorter LRRC8C^{t379}, the longer LRRC8C^{t419} elutes at a similar volume as LRRC8C^{trunc}. (**C**) Mean current density (at 100 mV) of LRRC8$^{-/-}$ cells transfected with constructs coding for LRRC8A and either LRRC8C^{t419} ($n = 5$) or LRRC8C^{t419} ($n = 8$) recorded by patch-clamp electrophysiology in the whole-cell configuration in isotonic (measured 10 s after establishment of whole-cell configuration) and hypotonic conditions (measured 4 min after switch to hypotonic solutions) in buffer system 1 (Δsalt). Panels show measurements of individual cells (spheres), bars represent mean currents, errors are s.e.m. Mean current densities obtained from LRRC8A/C^{WT} (red) and LRRC8A/C^{trunc} channels (blue, obtained from Fig. 4G) are shown as dashed line for comparison. Deviations of currents of both constructs to WT and mutated LRRC8C in the respective conditions were evaluated by a Brown–Forsythe and Welch's ANOVA test with Dunnett's T3 multiple comparison testing. Deviations between isotonic and hypotonic conditions for each construct was separately evaluated by unpaired *t* testing with Welsch's correction applied. Differences to LRRC8A/C^{WT} were in all cases found to be not statistically significant (LRRC8A/C^{t379} isotonic, $P = 0.542$, hypotonic, $P = 0.302$; LRRC8A/C^{t419} isotonic, $P = 0.236$, hypotonic, $P = 0.366$). Differences to LRRCA/C^{trunc} were evaluated as significant (LRRC8A/C^{t379} isotonic, $P = 0.0023$, hypotonic, $P = 0.0028$; LRRC8A/C^{t419} isotonic, $P = 0.0002$, hypotonic, $P = 0.0003$). Current increases of both constructs upon change to hypotonic conditions were evaluated as statistically not significant (LRRC8A/C^{t379} $P = 0.274$; LRRC8A/C^{t419}, $P = 0.113$).

